Supplement to: PhotoSpec: A New Instrument to Measure Spatially Distributed Red and Far-Red Solar-Induced Chlorophyll Fluorescence

Katja Grossmann[a,b], Christian Frankenberg[c,d], Troy S. Magney[c,d], Stephen C. Hurlock[a,b], Ulrike Seibt[a], Jochen Stutz[a,b,*]

[a] *Department of Atmospheric and Oceanic Sciences, University of California Los Angeles, Los Angeles, CA, USA*
[b] *Joint Institute for Regional Earth System Science and University of California Los Angeles, Los Angeles, CA, USA*
[c] *Division of Geological and Planetary Sciences, California Institute of Technology, Pasadena, CA, USA*
[d] *NASA Jet Propulsion Laboratory, California Institute of Technology, Pasadena, CA, USA*

[*] Corresponding author
Email address: jochen@atmos.ucla.edu (Jochen Stutz)

Contents

S1. Theory

This section explains the derivation of Equation 2 from Section 2 (*Theory*), Equation 6 from Section 2.1.1 (*Linearized retrieval in an ideal case*), and Equation 9 and 10 from Section 2.2.1 (*Detector nonlinearity*).

S1.1. Derivation of Equation 2

The change in optical density due to the additive emission by SIF can be derived as follows:

$$
\begin{aligned}
\ln\left(\frac{I^{\mathrm{C}}}{I_0^{\mathrm{C}}}\right) &= \ln\left(\frac{a^{\mathrm{C}} \cdot I + I_{\mathrm{SIF}}}{a^{\mathrm{C}} \cdot I_0 + I_{\mathrm{SIF}}}\right) \\
&= \ln\left(a^{\mathrm{C}} \cdot I\right) + \ln\left(1 + \frac{I_{\mathrm{SIF}}}{a^{\mathrm{C}} \cdot I}\right) - \ln(a^{\mathrm{C}} \cdot I_0) \\
&\quad - \ln\left(1 + \frac{I_{\mathrm{SIF}}}{a^{\mathrm{C}} \cdot I_0}\right), \quad \text{with } \ln(1+x) \approx x \\
&\approx \ln\left(\frac{I}{I_0}\right) + \frac{I_{\mathrm{SIF}}}{a^{\mathrm{C}} \cdot I} - \frac{I_{\mathrm{SIF}}}{a^{\mathrm{C}} \cdot I_0} \\
&= \ln\left(\frac{I}{I_0}\right) + \frac{I_{\mathrm{SIF}}}{a^{\mathrm{C}} \cdot I_0} \cdot \left(\frac{I_0}{I} - 1\right) \\
&\quad \text{with } \ln(1+x) \approx x \quad \text{and} \quad x = I_0/I - 1 \\
&\approx \ln\left(\frac{I}{I_0}\right) + \frac{I_{\mathrm{SIF}}}{a^{\mathrm{C}} \cdot I_0} \cdot \ln\left(\frac{I_0}{I}\right) \\
&= \ln\left(\frac{I}{I_0}\right) \cdot \left(1 - \frac{I_{\mathrm{SIF}}}{a^{\mathrm{C}} \cdot I_0}\right).
\end{aligned}
\tag{S1}
$$

S1.2. Derivation of Equation 6

The linearization follows the general approach common for trace gas retrievals in solar spectra, i.e., it is performed on the natural logarithm of the intensities using a Taylor series of the logarithm with $O(x^2)$ representing higher orders of

this approximation:

$$\begin{aligned}
\ln(I^{\mathrm{C}}(\lambda)) &= \ln(a^{\mathrm{C}}(\lambda)\cdot I(\lambda) + I_{\mathrm{SIF}}(\lambda)) \\
&= \ln(a^{\mathrm{C}}(\lambda)\cdot I(\lambda)) + \ln\left(1 + \frac{I_{\mathrm{SIF}}(\lambda)}{a^{\mathrm{C}}(\lambda)\cdot I(\lambda)}\right) \\
&\quad \text{with } \ln(1+x) \approx x + O(x^2) \\
&\approx \ln(a^{\mathrm{C}}(\lambda)\cdot I(\lambda)) + \frac{I_{\mathrm{SIF}}(\lambda)}{a^{\mathrm{C}}(\lambda)\cdot I(\lambda)} \quad \text{with } I^{\mathrm{C}}(\lambda) \approx a^{\mathrm{C}}(\lambda)\cdot I(\lambda) \\
&\approx \ln(I^{\mathrm{D}}(\lambda)) + \ln\left(\frac{a^{\mathrm{C}}(\lambda)}{a^{\mathrm{D}}(\lambda)}\right) + \frac{I_{\mathrm{SIF}}(\lambda)}{I^{\mathrm{C}}(\lambda)}.
\end{aligned} \tag{S2}$$

Equation S2 includes two approximations which need to be discussed in more detail. The first is the approximation of the logarithm. We can use the second term of the Taylor expansion of $\ln(1+x) = x - x^2/2 + O(x^3)$ as the error of this approximation. Typical values of $\frac{I_{\mathrm{SIF}}(\lambda)}{I^{\mathrm{C}}(\lambda)}$ in the far-red wavelength range are 0 - 0.03. Consequently, this approximation leads to a positive bias in $\frac{I_{\mathrm{SIF}}(\lambda)}{I^{\mathrm{C}}(\lambda)}$ of 0 - $4.5 \cdot 10^{-4}$ or, expressed in relative terms, it imposes a positive relative bias of 0 - 1.5% on $\frac{I_{\mathrm{SIF}}(\lambda)}{I^{\mathrm{C}}(\lambda)}$. The situation is, however, different in the red wavelength range where $\frac{I_{\mathrm{SIF}}(\lambda)}{I^{\mathrm{C}}(\lambda)}$ can be 0 - 0.3, due to the much lower canopy reflectivity in this wavelength range. The positive bias can thus be up to 10 times higher, introducing considerable errors in the retrieval. We will present a solution to this problem in Section 2.1.2 in the manuscript.

The second approximation is $I^{\mathrm{C}}(\lambda) \approx a^{\mathrm{C}} \cdot I(\lambda)$. We can rewrite the following term of this approximation using a Taylor expansion to quantify this error:

$$\begin{aligned}
\frac{I_{\mathrm{SIF}}(\lambda)}{a^{\mathrm{C}}\cdot I(\lambda)} &= \frac{I_{\mathrm{SIF}}(\lambda)}{I^{\mathrm{C}}(\lambda) - I_{\mathrm{SIF}}(\lambda)} \\
&= \frac{I_{\mathrm{SIF}}(\lambda)}{I^{\mathrm{C}}(\lambda)} \cdot \left(\frac{1}{1 - \frac{I_{\mathrm{SIF}}(\lambda)}{I^{\mathrm{C}}(\lambda)}}\right) \qquad \text{with} \qquad \frac{1}{1-x} = 1 + x + x^2 + \dots \\
&= \frac{I_{\mathrm{SIF}}(\lambda)}{I^{\mathrm{C}}(\lambda)} \cdot \left(1 + \frac{I_{\mathrm{SIF}}(\lambda)}{I^{C}(\lambda)} + \left(\frac{I_{\mathrm{SIF}}(\lambda)}{I^{\mathrm{C}}(\lambda)}\right)^2 + \dots\right).
\end{aligned} \tag{S3}$$

The error is thus approximately $\left(\frac{I_{\mathrm{SIF}}(\lambda)}{I^{\mathrm{C}}(\lambda)}\right)^2$. For typical values of $\frac{I_{\mathrm{SIF}}(\lambda)}{I^{\mathrm{C}}(\lambda)}$ of 0 - 3%, this approximation leads to a negative bias in $\frac{I_{\mathrm{SIF}}(\lambda)}{I^{\mathrm{C}}(\lambda)}$ of 0 - $9 \cdot 10^{-4}$, i.e., it imposes a negative bias of 0 - 3% on $\frac{I_{\mathrm{SIF}}(\lambda)}{I^{\mathrm{C}}(\lambda)}$. As in the first approximation, the larger $\frac{I_{\mathrm{SIF}}(\lambda)}{I^{\mathrm{C}}(\lambda)}$ in the red wavelength range again leads to a much higher bias. It is interesting

to note that the two approximations are of opposite sign and thus partly cancel each other. Combining both approximations leads to a negative bias in $\frac{I_{\mathrm{SIF}}(\lambda)}{I^{\mathrm{D}}(\lambda)}$ of 0 - $4.5 \cdot 10^{-4}$ or, expressed in relative terms, it imposes a positive bias of 0 - 1.5% on $\frac{I_{\mathrm{SIF}}(\lambda)}{I^{\mathrm{D}}(\lambda)}$, in the far-red wavelength range. As with the first approximation, the bias in the red wavelength range is considerably higher, i.e. 0 - 15% on $\frac{I_{\mathrm{SIF}}(\lambda)}{I^{\mathrm{D}}(\lambda)}$.

S1.3. Derivation of Equation 9

Using the definitions introduced in Equation 8 of the manuscript, we can define the optical depth of the Fraunhofer band as:

$$\begin{aligned}
\ln\left(\frac{I}{I_0}\right) &= \ln\left(\frac{d_1 \cdot F \cdot L_0 + d_2 \cdot F^2 \cdot L_0^2}{d_1 \cdot L_0 + d_2 \cdot L_0^2}\right) \qquad \text{with} \quad F = \frac{L}{L_0} \\
&= \ln(d_1 \cdot F \cdot L_0) + \ln\left(1 + \frac{d_2 \cdot F^2 \cdot L_0^2}{d_1 \cdot F \cdot L_0}\right) - \ln(d_1 \cdot L_0) \\
&\quad + \ln\left(1 + \frac{d_2 \cdot L_0^2}{d_1 \cdot L_0}\right) \qquad \text{with } \frac{d_2}{d_1} \text{ small} \\
&\approx \ln(F) + \frac{d_2}{d_1} \cdot F \cdot L_0 - \frac{d_2}{d_1} \cdot L_0 \\
&= \ln(F) + \frac{d_2}{d_1} \cdot L_0 \cdot (F - 1) \qquad \text{with NL} = \frac{d_2 \cdot L_0^2}{d_1 \cdot L_0} = \frac{d_2}{d_1} \cdot L_0 \\
&= \ln(F) - \mathrm{NL} \cdot (1 - \mathrm{F}).
\end{aligned} \tag{S4}$$

NL is the relative nonlinearity which determines the deviation based on the linearity from the ratio of the quadratic and linear terms.

S1.4. Derivation of Equation 10

$$\begin{aligned}
\ln\left(\frac{I + I_{\mathrm{SIF}}}{I_0 + I_{\mathrm{SIF}}}\right) &= \ln\left(\frac{I}{I_0}\right)\left(1 - \frac{I_{\mathrm{SIF}}}{I_0}\right) \\
&= \ln(F) - \ln(F) \cdot \frac{I_{\mathrm{SIF}}}{I_0} \\
&\approx \ln(F) - (1 - F) \cdot \frac{I_{\mathrm{SIF}}}{I_0}.
\end{aligned} \tag{S5}$$

S2. Radiometric calibration

The radiometric calibration is different for each PhotoSpec system and for each field site. Thus, the radiometric calibration has to be performed for each instrument and at each field site. The radiometric calibration measurements are preferably made around noon and when it is cloud-free for at least 15-30 minutes. The calibrated spectrometer and the PhotoSpec system are temporally synced and record spectra simultaneously. Figure S1 shows an example of the calibration results for the field site at Niwot Ridge, Colorado on 10/17/2017. The SIF calibration factor is the average value of this calibration factor in the SIF retrieval wavelength range for the red (680 - 686 nm) and far-red (745 - 758 nm) wavelength range.

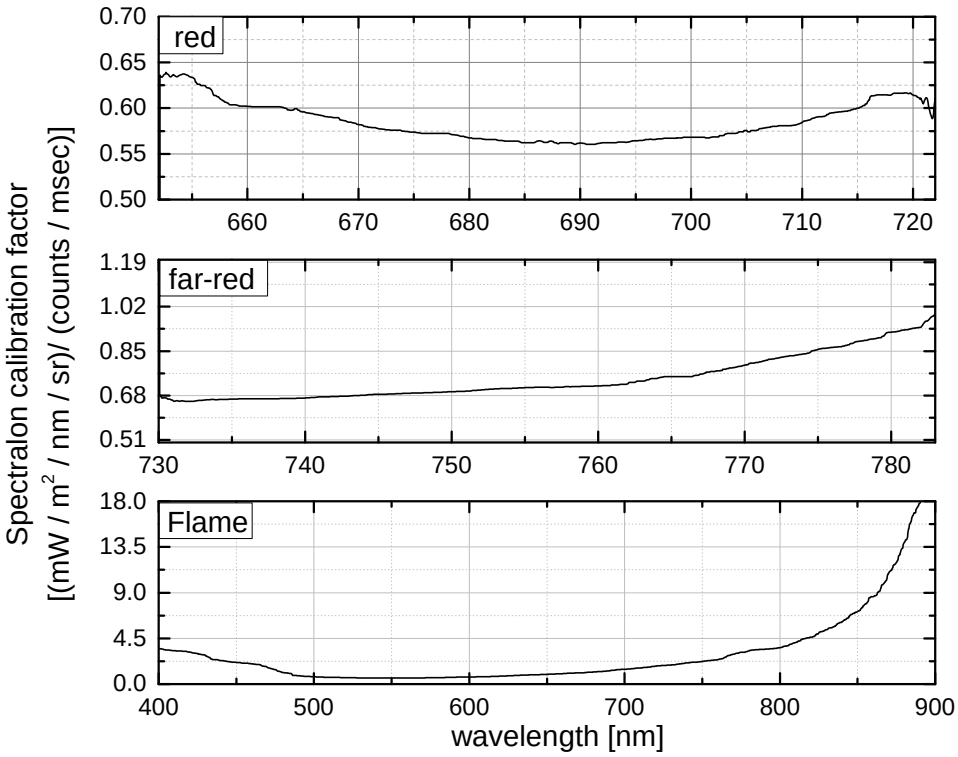

Figure S1: Spectralon calibration factors for the three PhotoSpec spectrometers for the field site at Niwot Ridge, Colorado recorded on 10/17/2017.

Figure S2 shows the radiances of a soil and pine tree spectrum recorded with

the PhotoSpec Flame spectrometer and calibrated with the calibration factor from Figure S1.

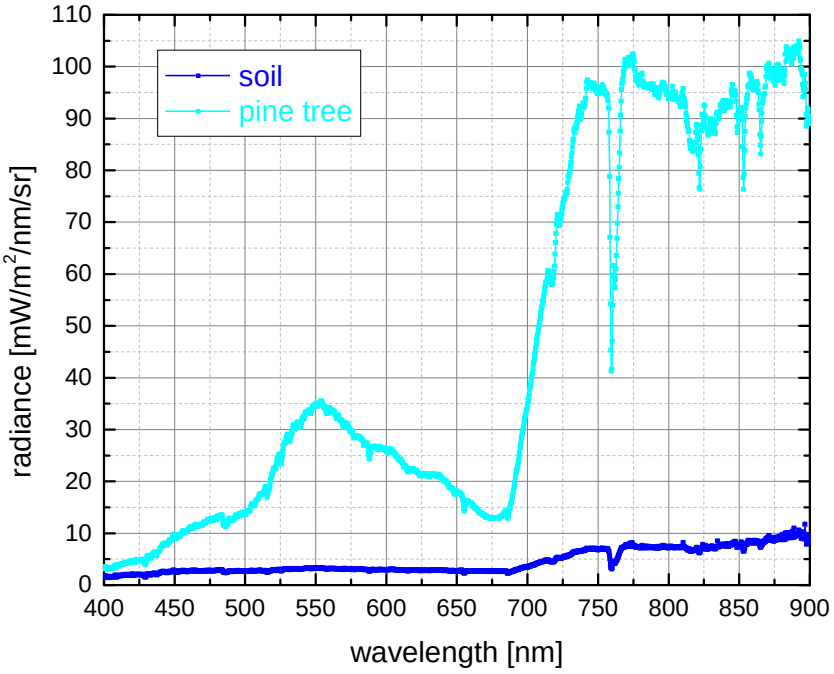

Figure S2: Flame radiances of a soil and pine tree target at Niwot Ridge, Colorado on 6/26/2017 calculated using the calibration factors from Figure S1.

S3. PAM measurements

The SIF measurements on the roof of the UCLA Math Sciences building were compared to field observations using a portable chlorophyll fluorometer (PAM-2500, Heinz Walz GmbH, Effeltrich, Germany) to link the SIF signal to fluorescence yields (F_t and F_m from PAM). Leaf scale measurements of fluorescence have been carried out for decades using pulse amplitude modulation (PAM) fluorometers (e.g., Genty et al., 1989; Krause and Weis, 1991; Pfündel, 1998; Baker, 2008; Porcar-Castell et al., 2014) to simultaneously measure chlorophyll fluorescence and photosynthetic CO_2 uptake of individual leaves (e.g., Flexas et al., 1999; Rascher et al., 2000; Magney et al., 2017). The pulse amplitude-modulated (PAM)

technique is an active technique that involves the use of a measuring light and a saturating light pulse with a leaf clip holder (Schreiber et al., 1986; Bilger et al., 1995; Schreiber, 2004). The PAM-2500 fluorometer (`http://www.walz.com`) is mainly used for measurements of the effective quantum yield (dF/F'_{m}) of photosystem II (PS II) under ambient light conditions and for measurements of the potential quantum yield ($F_{\mathrm{V}}/F_{\mathrm{m}}$) of dark-adapted samples (Rascher et al., 2000). The PAM technique is restricted to the leaf level and cannot be applied to the canopy and landscape levels. The sample leaf was attached to a mount to avoid movements of the leaf, for example due to wind. The leaf was oriented in the horizontal direction in order to mimimize shading. The PAM-2500 leaf clip was attached to one side of the leaf, next to, but outside, of the spot covered by the FOV of the PhotoSpec telescope. In order to measure the effective quantum yield of PSII, saturating light pulses were triggered every five minutes. The effective quantum yield of PSII was measured by the PAM-2500 fluorometer and is determined according to:

$$\frac{dF}{F'_{\mathrm{m}}} = \frac{F'_{\mathrm{m}} - F}{F'_{\mathrm{m}}}, \tag{S6}$$

with F being the fluorescence yield of the light-adapted sample and F'_{m} being the maximum light-adapted fluorescence yield when a saturating light pulse is superimposed on the ambient light levels.

S4. Non-fluorescence targets

Figure S3 shows the diurnal cycle of the SIF signal of soil as an example for a non-fluorescence target compared to a pine tree at Niwot Ridge, Colorado. The soil SIF signal varies around 0 mW $\mathrm{m^{-2}sr^{-1}nm^{-1}}$ with approximately ±0.03 mW $\mathrm{m^{-2}sr^{-1}nm^{-1}}$.

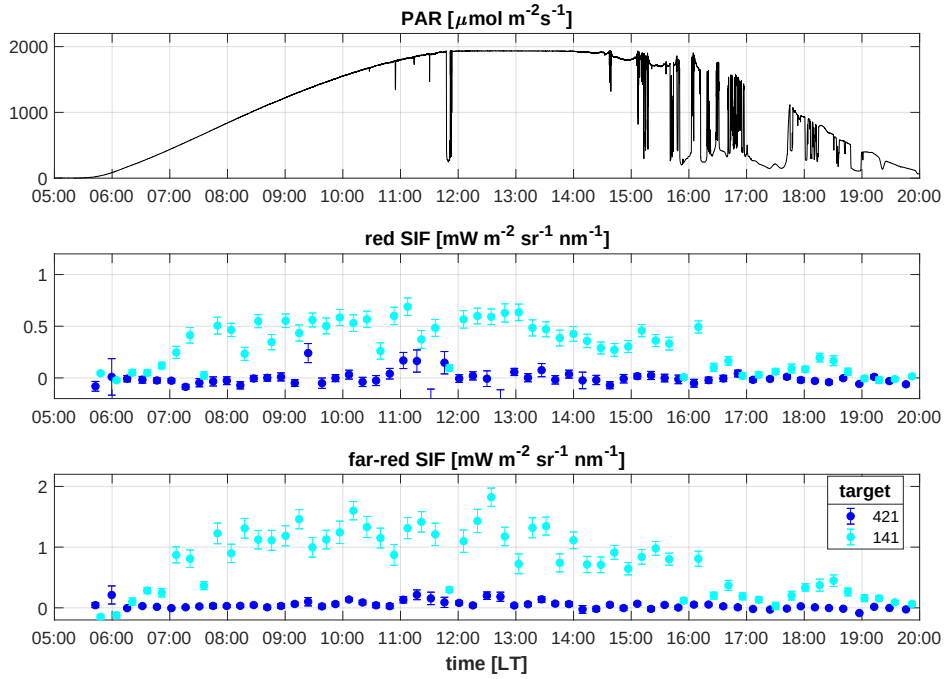

Figure S3: Diurnal cycle of (a) PAR, (b) red SIF, and (c) far-red SIF for soil (blue) and a pine tree (turquoise) observed from a 26 m tower at Niwot Ridge, Colorado on 6/26/2017.

Baker, N. R., 2008. Chlorophyll fluorescence: A probe of photosynthesis in vivo. Annu. Rev. Plant Biol. 59 (1), 89–113.

Bilger, W., Schreiber, U., Bock, M., 1995. Determination of the quantum efficiency of photosystem II and of non-photochemical quenching of chlorophyll fluorescence in the field. Oecologia 102 (4), 425–432.

Flexas, J., Escalona, J. M., Medrano, H., 1999. Water stress induces different levels of photosynthesis and electron transport rate regulation in grapevines. Plant, Cell & Environment 22 (1), 39–48.

Genty, B., Briantais, J.-M., Baker, N. R., 1989. The relationship between the quantum yield of photosynthetic electron transport and quenching of chlorophyll fluorescence. Biochim. Biophys. Acta 990 (1), 87 – 92.

Krause, G., Weis, E., 1991. Chlorophyll fluorescence and photosynthesis: The basics. Ann. Rev. Plant Phys. Plant Mol. Biol. 42 (1), 313–349.

Magney, T. S., Frankenberg, C., Fisher, J. B., Sun, Y., North, G. B., Davis, T. S., Kornfeld, A., Siebke, K., 2017. Connecting active to passive fluorescence with photosynthesis: a method for evaluating remote sensing measurements of Chl fluorescence. New Phytol.2017-23758.

Pfündel, E., 1998. Estimating the contribution of photosystem I to total leaf chlorophyll fluorescence. Photosynth. Res. 56 (2), 185–195.

Porcar-Castell, A., Tyystjärvi, E., Atherton, J., van der Tol, C., Flexas, J., Pfündel, E. E., Moreno, J., Frankenberg, C., Berry, J. A., 2014. Linking chlorophyll a fluorescence to photosynthesis for remote sensing applications: mechanisms and challenges. J. Exp. Bot. 65 (15), 4065–4095.

Rascher, U., Liebig, M., Lüttge, U., 2000. Evaluation of instant light-response curves of chlorophyll fluorescence parameters obtained with a portable chlorophyll fluorometer on site in the field. Plant, Cell and Environment 23 (12), 1397–1405.

Schreiber, U., 2004. Pulse-Amplitude-Modulation (PAM) fluorometry and saturation pulse method: An overview. Springer Netherlands, Dordrecht, pp. 279–319.

118 Schreiber, U., Schliwa, U., Bilger, W., 1986. Continuous recording of photo-
119 chemical and non-photochemical chlorophyll fluorescence quenching with a
120 new type of modulation fluorometer. Photosynth. Res. 10 (1), 51–62.